Original scientific paper

Synthesis and electrochemical characterization of sulfur-doped Li₃PO₄ for all-solid-state battery applications

Hany El-Shinawi^✉ and Shady M. El-Dafrawy

Department of Chemistry, Faculty of Science, Mansoura University, Mansoura, 35516, Egypt

Corresponding authors: ✉*h_elshinawi@mans.edu.eg; tel.: +20502327236*

Abstract

Isovalent and aliovalent cation-doping have been widely investigated to enhance ion transport in γ-Li₃PO₄-type lithium superionic conductors (LISICONs). Anion doping, however, has been restricted to a full replacement of oxide ions by sulfide ions in some compounds (the so-called thio-LISICONs). The replacement of oxide ions by sulfide ions enhances both ion conductivity and deformability of the materials. Similar to other sulfide-type solid-electrolytes, thio-LISICONs, however, showed limited electrochemical stability against oxidation. In this report, a sonication-assisted liquid-phase synthesis approach was employed to achieve substantial sulfur-oxygen mixing in γ-type Li₃PO₄. Sulfur-doped Li₃PO₄ possessed an ion conductivity four orders of magnitude higher than that of γ-Li₃PO₄, and a notably low activation energy of ion transport of 0.40(8) eV. Sulfur-oxygen mixing in sulfur-doped Li₃PO₄ enhanced electrochemical stability against oxidation (up to 4 V vs. Li⁺/Li) compared with sulfur-based Li₃PS₄. This study paves the way for developing mixed-anion phases in the γ-type Li₃PO₄ structure with enhanced electrochemical properties for all-solid-state battery applications.

Keywords
Lithium-ion battery; solid-state electrolyte; lithium superionic conductor; ionic conductivity; anion doping

Introduction

All-solid-state Li-ion batteries allow safer and more reliable energy storage compared to conventional Li-ion batteries [1]. A Li-ion solid-state electrolyte is a key component in these batteries. In addition to fast ion conduction, a promising solid-state electrolyte for all-solid-state battery applications will have good mechanical properties that enable a facile formulation of bulk-type solid-state cells and good electrochemical stability (in contact with high-voltage cathodes and/or Li anodes) that enables stable and high performance of the cells [1,2]. Oxide-type solid electrolytes such as LISICONs, NASICONs and lithium garnets possess enhanced electrochemical

stability windows compared with other types of solid electrolytes such as sulfides [3,4], which offers more opportunities to realize stable, high-performing all-solid-state cells. While sulfides are ductile and easily form dense cathode composites by cold/warm pressing, oxides are brittle and often experience mechanical failure through cracking. Efforts have been devoted in the last few decades to improving Li-ion conductivity in different oxides [5,6], with aliovalent doping being the main approach in these studies. Manipulating the deformability of Li-ion conducting oxides has also recently received considerable interest in literature [7,8].

γ-Li$_3$PO$_4$-type lithium superionic conductors (LISICONs) form an important family of oxide-type solid electrolytes, which have been extensively studied. Isovalent and aliovalent doping in this system enables an enhancement of the ion conductivity from < 10^{-10} S cm^{-1} in parent materials (*e.g.* Li$_3$PO$_4$, Li$_3$VO$_4$, Li$_4$GeO$_4$ and Li$_4$SiO$_4$) to ~10^{-6} S cm^{-1} in mixed-cation systems [9-11]. Optimum conductivities have recently been reported in complex cation systems such as Li$_{3.53}$(Ge$_{0.75}$P$_{0.25}$)$_{0.7}$V$_{0.3}$O$_4$ [9] and Li$_{3.68}$(Ge$_{0.6}$V$_{0.36}$Ga$_{0.04}$)O$_4$ [11]. Like other oxide-type solid electrolytes, LISICONs are stiff ceramics and difficult to integrate into practical all-solid-sate batteries. Another approach to manipulate both ion conductivity and mechanical properties of LISICONs is to dope the materials at the oxygen sites. A full replacement of oxide ions by softer anions such as sulfide ions has been achieved in the so-called thio-LISICONs [12,13], which showed enhanced ion conductivities and good deformability. Thio-LISICONs, however, similar to other sulfide-type solid electrolytes [3], are not compatible with conventional cathodes due to limited electrochemical stability at high and moderate voltages. These findings have motivated a search for new phases with good ion transport properties and considerable electrochemical stability. One approach is the development of mixed-anion phases. Oxygen doping in β-type Li$_3$PS$_4$, for example, has been suggested by calculations [14-16] to enhance the electrochemical properties of Li$_3$PS$_4$. However, a few examples of this doping have been realized by experiment [17-20]. In these experimental studies, phases with small oxygen contents that adopt either β-type Li$_3$PS$_4$ structure or Li$_{10}$GeP$_2$S$_{12}$ (LGPS)-type structure have been achieved [17-20]. These studies also revealed a great challenge in synthesizing these materials, which is often non-scalable and results in multiple phases. To the best of our knowledge, very limited success has been achieved in developing mixed oxide-sulfide phases with γ-Li$_3$PO$_4$ LISICON-type structure. Here, we report a liquid-phase synthesis approach of sulfur-doped γ-Li$_3$PO$_4$. Liquid-phase synthesis enhances the scalability of the synthesis process and allows the formation of novel phases at low-temperature sintering [21,22]. The synthesized sulfur-doped γ-Li$_3$PO$_4$ possessed good deformability and can be densified by cold-pressing, enabling ion conductivity that is several orders of magnitude higher than that of the parent γ-Li$_3$PO$_4$ compound. Sulfur-doped γ-Li$_3$PO$_4$ also showed enhanced electrochemical stability compared with the sulfur-based β-Li$_3$PS$_4$ compound.

Experimental

Synthesis

Lithium sulfide and phosphorus pentoxide were used as starting materials to synthesize sulfur-doped Li$_3$PO$_4$. The two materials were mixed in 3:1 molar ratio in tetrahydrofuran (THF) in an argon-filled glovebox. The solid materials to solvent ratio of the mixture was ~0.04 g/ml. The mixture was stirred at room temperature for 4 days with intermediate sonication steps (for a total of ~16h). The THF solvent was then removed by evaporation at 80 °C, and the solid precursor was further dried under vacuum at 80 °C for 12 h. The solid precursor was then heated under argon at 400 °C for 24 h and stored in argon-filled glovebox.

Characterizations

X-ray powder diffraction (XRD) data were collected using a PANalytical X'Pert PRO diffractometer in a reflection mode and using Cu-Kα radiation. Scanning electron microscopy (SEM) and energy dispersive X-ray spectroscopy (EDX) studies were performed using an FEI Inspect F50 electron microscope. IR spectra were recorded using a Shimadzu IR affinity spectrophotometer. Electrochemical impedance spectroscopy (EIS) studies were performed on cold-pressed pellets, employing very thin Al-foil discs as electrodes. The measurements were conducted in Swagelok cells assembled under an argon atmosphere, and the data were recorded using a Biologic SP-150 Potentiostat. Prior to each AC impedance measurement, the cells were equilibrated at the same temperature for one hour and then data were recorded in the frequency range of 1 MHz to 1 Hz, with an electrical perturbation of 40 mV. To test the electrochemical stability window of the studied materials, asymmetric cells of In/SE/SE-C were constructed by cold pressing (SE is either sulfur-doped Li_3PO_4 or Li_3PS_4). SE-C composites were initially prepared by mixing either sulfur-doped Li_3PO_4 or Li_3PS_4 with carbon black (15 wt.%) using a pestle and mortar. Three-layer cells of indium foil, 80 mg SE and 3 mg of the SE-C composite were uniaxially pressed at ~250 MPa for 30 s. Indium foil was thinned (on a thin Cu-foil disc) before use. Thin Cu-foil and Al-foil discs were employed to support the cell and to collect the current from the anode and the cathode sides, respectively. The assembled cells were studied by cyclic voltammetry (CV) in Swagelok cells at 80 °C using a BioLogic VMP-300 Potentiostat, using a scan rate of 0.1 mV s^{-1} in the voltage range 0-2.6 V *vs.* In/InLi (~0.6-3.2 V *vs.* Li$^+$/Li). The room temperature equilibrium redox potential of the In/InLi electrode within the (In−InLi) two-phase region (or, more precisely, the Li$^+$/(In−InLi) electrode) is 0.62 V *vs.* Li$^+$/Li [23].

Results and discussion

Solvent-mediated reactions (or the so-called liquid-phase synthesis) have recently been proposed as a facile, scalable approach to synthesize Li-ion solid-state electrolytes such as sulfides [21]. One of the earliest examples of these reactions is the reaction between Li_2S and P_2S_5 in THF to prepare fast-ion conducting β-type Li_3PS_4 [22]. Our attempts to achieve substantial sulfur-oxygen mixing in Li_3PO_4 by reacting Li_2S and P_2O_5 in THF were initially hindered by the slow kinetics of the reaction due to relative inertness of P_2O_5 compared with P_2S_5. Li *et al*. [24], for example, have reported an effect of small P_2O_5 proportions (1-5 mol %) on the crystallite sizes of β-type Li_3PS_4 synthesized by reacting P_2S_5 and Li_2S in THF, with no direct evidence of appreciable oxygen incorporation in the material. In this study, the reaction between Li_2S and P_2O_5 in THF was accelerated by ultrasonic irradiation, leading to a substantial mixing of sulfur and oxygen in Li_3PO_4. Figure 1 shows SEM images of the reaction mixture at different reaction stages. During the course of the reaction, micrometer-sized P_2O_5 particles are gradually converted into nanostructured architectures of a new mixed oxygen-sulfur phase. The oxygen-to-sulfur ratio in this phase, as approximately determined by EDX, was dependent on the lifetime of the reaction, with a significant degree of inhomogeneity throughout the material. By the end of the reaction, the nanostructured mixed oxygen-sulfur phase has become the predominant component of the material, leading to a more homogenous phase (denoted as LPOS) with an approximate oxygen-to-sulfur atomic ratio of ~69:31 (Figure 1c). This ratio is close to the initial stoichiometry of the starting materials (1P_2O_5:3Li_2S; *i.e.,* O:S atomic ratio of 62.5:37.5), which indicates that the liquid-phase reaction step has been successful in homogenizing the reacting species in a single solid precursor. XRD analysis indicated that this solid precursor was amorphous. The material was therefore heated under argon at 400 °C (argon-calcined LPOS) to enhance phase formation.
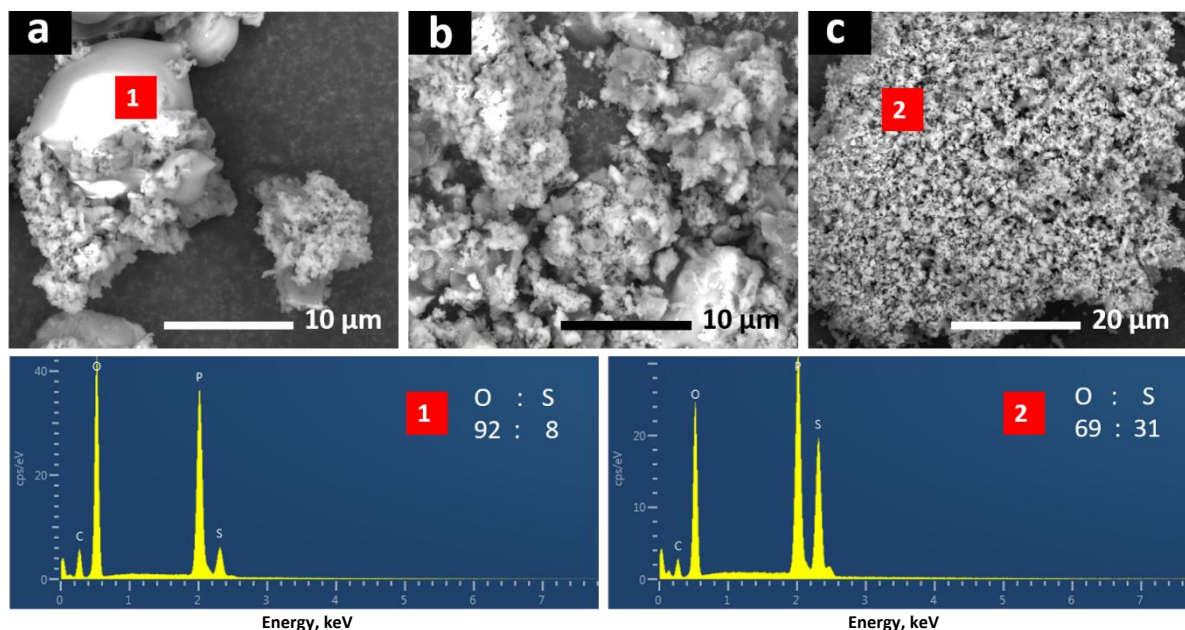
***Figure 1**. SEM images collected from the liquid-phase reaction mixture during the course of the reaction (4 days), and corresponding EDX analyses indicating O:S atomic ratios. a) SEM image collected after ~24 h showing micrometer-sized P_2O_5 particles being converted into a nanostructured architecture of a mixed O-S phase; b) SEM image collected after 2 days; c) SEM image collected after 4 days*

The XRD pattern collected from argon-calcined LPOS is shown in Figure 2. A sample of LPOS was also calcined in air at 400 °C and the XRD pattern is presented in Figure 2 for comparison. Air-calcined LPOS showed an XRD pattern characteristic of γ-Li_3PO_4 [25]. Peak broadening is clearly associated with the nanostructured morphology of the material [8,26]. The argon-calcined sample, interestingly, showed a related XRD pattern with a significant peak shift towards lower angles. A larger lattice in the case of argon-calcined LPOS, hence, is attributed to the incorporation of sulfur in Li_3PO_4. The observed peak broadening/overlapping in argon-calcined LPOS is associated with the nanostructured morphology of the material [8,26] and/or the presence of residues of Li_3PO_4 [25] in the material.
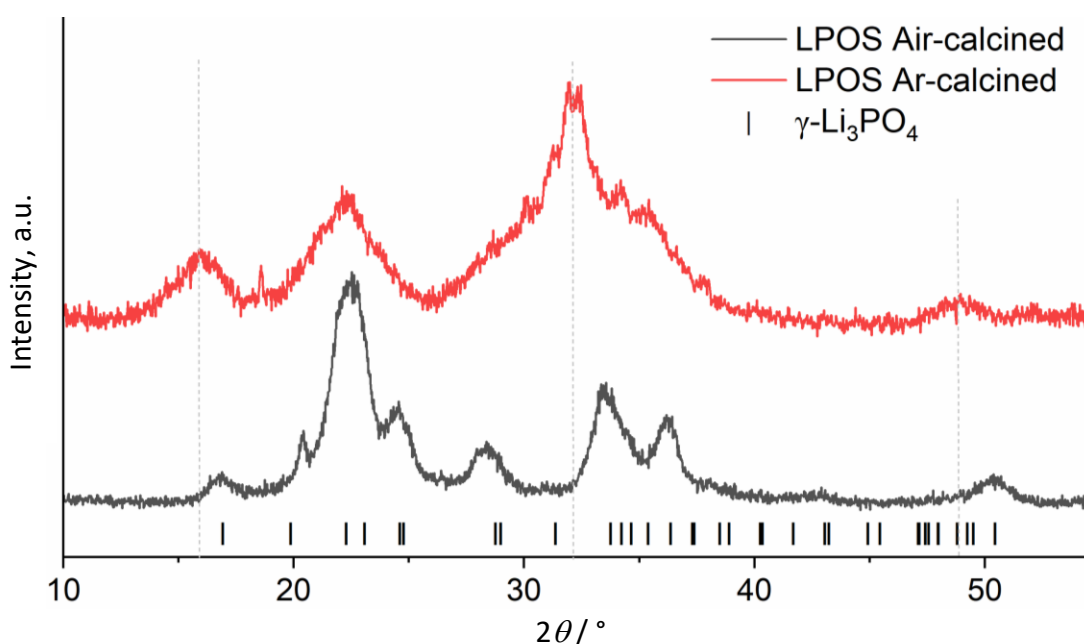
***Figure 2**. XRD patterns collected from LPOS samples after calcination in argon and in air (400°C). The black markers correspond to reflections from γ-Li_3PO_4 acording to [24]*

The materials were additionally examined by FTIR spectroscopy to investigate their local structure. Figure 3 shows the IR spectra of argon-calcined and air-calcined LPOS materials. The IR spectrum collected from (sulfur-based) β-type Li_3PS_4 is also presented for comparison. The spectrum of Li_3PS_4 consisted of a strong band at 560 cm^{-1}, which is assigned to the v_3 asymmetric stretching mode of the PS_4^{-3} group [27]. On the other hand, the spectrum of air-calcined LPOS displayed characteristic peaks of the vibrational modes of the PO_4^{-3} group. The strong peaks observed at 1033 and 600 cm^{-1} are well assigned to v_3 asymmetric stretching and v_4 bending modes of the PO_4^{-3} group, respectively [28,29]. These results are consistent with the XRD data, which suggest the formation of γ-Li_3PO_4 upon heating LPOS in air. In argon-calcined LPOS, the peak corresponding to the v_4 bending mode splits into two overlapping peaks at 595 and 612 cm^{-1}. This can be attributed to a site effect [28] due to sulfur's replacement of some oxygen in LPOS. The peak at 1033 cm^{-1} diminishes and a stronger (broader) peak is observed at ~970 cm^{-1}. The small peak at 1033 cm^{-1} may be attributed to a secondary phase of Li_3PO_4 in LPOS consistent with the XRD results, while we attribute the peak at 970 cm^{-1} to a stretching mode of mixed $P(O,S)_4^{-3}$ groups. These results are consistent with XRD and EDX analyses suggesting sulfur incorporation in γ-Li_3PO_4.
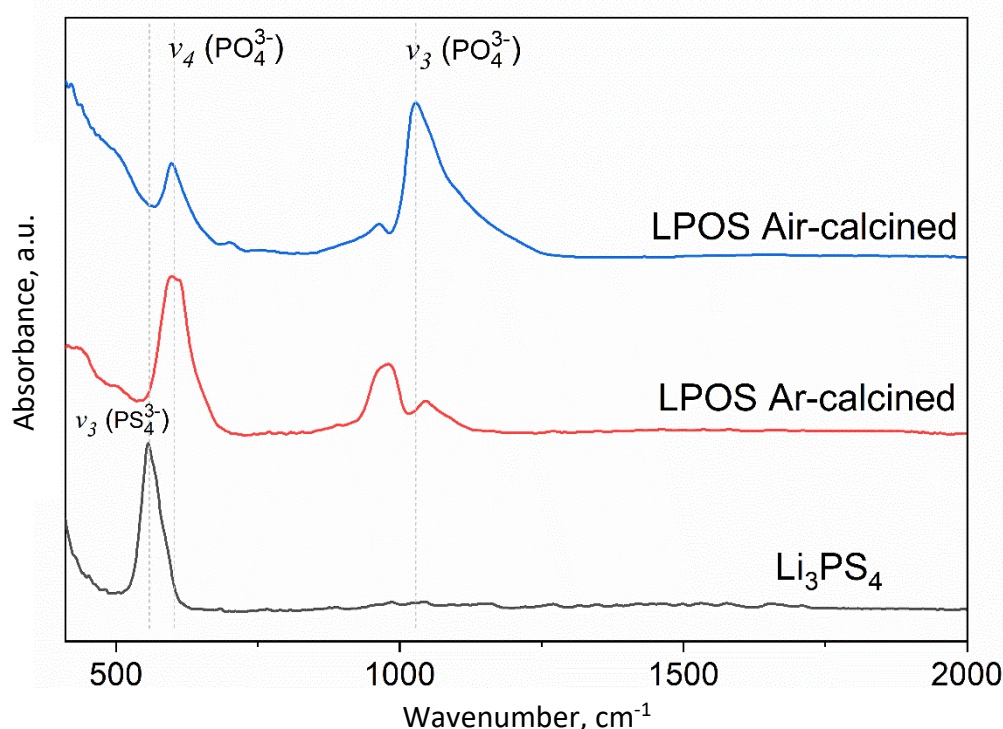
Figure 3. *FTIR spectra of sulfur-doped Li_3PO_4 (LPOS) and Li_3PS_4*

The effect of sulfur-doping on the ion transport properties of γ-Li_3PO_4 was examined by impedance spectroscopy. The use of a low-temperature synthesis route and the novel morphology of LPOS have enabled the densification of the material by cold pressing. The impedance spectra collected from cold-pressed pellets of the material (at ~250 MPa) are presented in Figure 4. A typical impedance spectrum of the material at 40 °C is shown in Figure 4b. The spectrum is composed of a distorted semicircle in the high to intermediate-frequency range and a low-frequency spike. The observation of a low-frequency spike is consistent with charge transport, which is mainly ionic and corresponds to Li-ion mobility. The distorted semicircle is assigned to the total resistance (bulk and grain-boundary resistances) of the material. The impedance data were fitted using a conventional [RQ]/[Q] equivalent circuit of the form [R1Q1][R2Q2]Q3, where [RQ] denotes a resistance

element (R) in parallel to a constant phase element (Q). The capacitances calculated from fitted Q1 and Q2 impedances are 46 and 150 pF, respectively. These values are consistent with contributions from the bulk and grain-boundary resistances, respectively [30]. The resistances R1 (632 kΩ) and R2 (304 kΩ) account for bulk and grain-boundary resistances, respectively, suggesting a total conductivity of the material of 0.15 μS cm⁻¹. The conductivity rises to 1.0 μS cm⁻¹ at 90 °C. Hence, the conductivity of LPOS is approximately four orders of magnitude higher than that of the parent γ-Li₃PO₄ compound (~0.10 nS cm⁻¹ at 100 °C [31]). The material is notably densified by cold-pressing, which gives LPOS an advantage over other doped Li₃PO₄ phases, considering its application in bulk-type all-solid-state Li-ion batteries. The observed grain-boundary resistance is smaller than the bulk resistance, which indicates an enhanced ion transport at the grain boundaries and a good sinterability of the material by cold-pressing. The activation energy (E_a) for the total conductivity of the material (σ) in the temperature range 20-90 °C (Figure 4a) is obtained from the Arrhenius plot of $\sigma = \sigma_0\,e^{-Ea/RT}$, where k is the Boltzmann constant, T is the absolute temperature and σ_0 is the pre-exponential factor. The Arrhenius plot is shown in Figure 4c, and suggests an activation energy of 0.40 eV. This value is significantly lower than that observed for parent γ-Li₃PO₄ (~1.1 eV [31]) and confirms enhanced ion transport properties in LPOS compared with the undoped material.
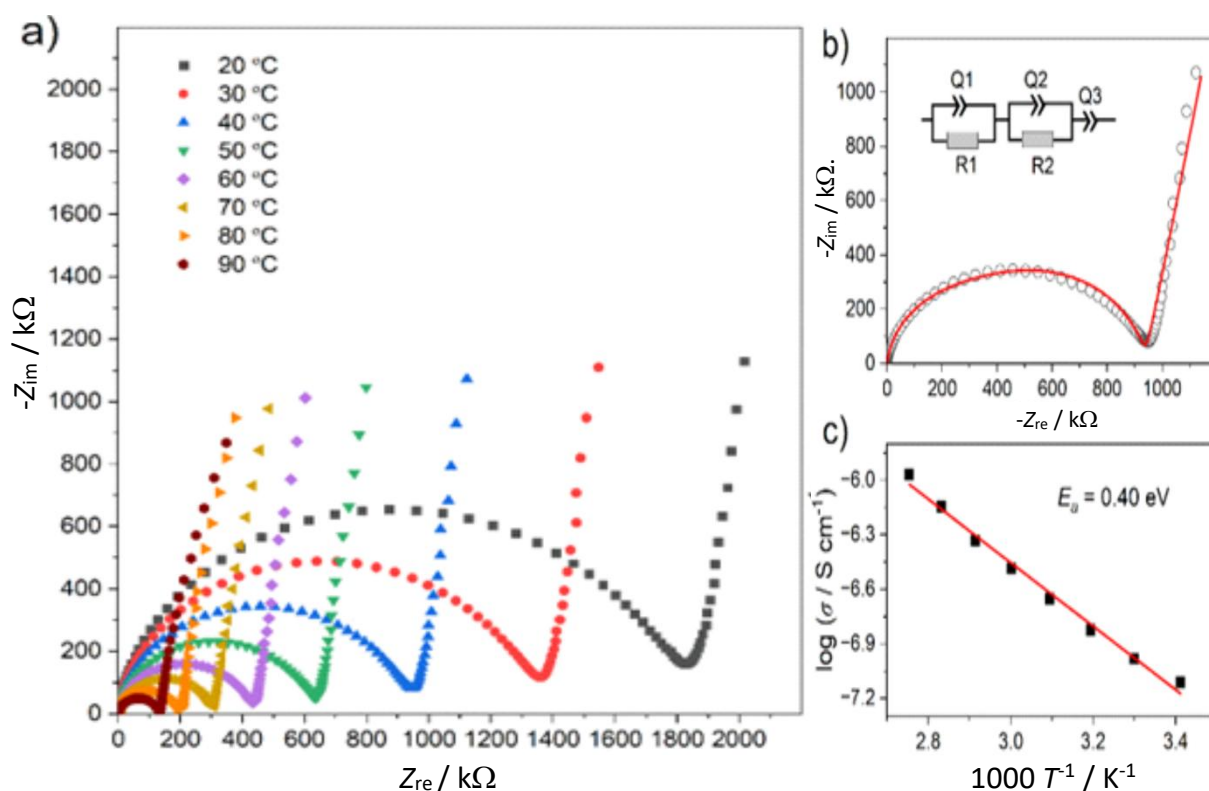

Figure 4. *a) Impedance spectra collected from argon-calcined LPOS at different temperatures; b) impedance plot of argon-calcined LPOS at 40 °C, fitted using the equivalent circuit shown in the inset; c) Arrhenius plot for the total conductivity of argon-calcined LPOS in the temperature range 20 to 90 °C*

The conductivity of LPOS is lower than that reported for sulfur-based compounds (thio-LISICONs) [12,13]. However, a mixed sulfide-oxide anion lattice in LPOS is expected to be more stable against oxidation than sulfide-based materials [14-20]. In order to confirm this hypothesis for sulfur-doped Li₃PO₄, the electrochemical stability of LPOS is investigated by cyclic voltammetry and compared with that of Li₃PS₄ (LPS). The asymmetric cells In/LPOS/LPOS-C and In/LPOS/LPS-C were investigated by stepwise cyclic voltammetry at 80 °C. The increased temperature was essential to enhance ion transport in LPOS. The use of LPOS-C and LPS-C composites as working electrodes

ensures large contact areas between LPOS/LPS and carbon, which allows a reliable estimation of the practical oxidative stability of the solid-electrolyte [32,33]. This setup is useful for investigating the electrochemical stability of the solid electrolytes suggested for use in Li-S batteries, where contact with carbon additives will be necessary. In the stepwise cyclic voltammetry technique [32], the potential is swept, starting from OCV, to a specific (oxidative) potential and then back to 0.0 V *vs.* In/InLi (0.6 V *vs.* Li$^+$/Li), and the cycle is ended at the OCV. For sulfur-based Li$_3$PS$_4$ (Figure 5), a reduction peak starts to evolve (at ~ 1.75 V and shifts to lower potentials) when the cut-off oxidative potential exceeds 2.1 V *vs.* In/InLi. This reduction peak is attributed to the redox activity of the decomposition products of Li$_3$PS$_4$ [32]. These results are in excellent agreement with previous studies, which suggest an oxidative stability limit of 2.2-2.3 V *vs.* In/InLi for Li$_3$PS$_4$ in similar setups [32]. LPOS, on the other hand, showed no evidence of decomposition in the same potential range. The stepwise cyclic voltammograms of LPOS (Figure 6) showed no evidence of significant redox activities in the scans up to 2.6 V *vs.* In/InLi (3.2 V *vs.* Li$^+$/Li). The superior stability of LPOS in contact with carbon in this potential range, compared with corresponding sulfides [32], makes the material useful as a solid-electrolyte in applications such as Li-S batteries. Stepwise cyclic voltam-mograms of LPOS at higher oxidative potentials (Figure 7) suggest good electrochemical stability of the material up to ~4 V *vs.* Li$^+$/Li. The scan up to 3.3 V *vs.* In/InLi showed no redox activities corresponding to the decomposition of the material, while the scans to 3.5 and 3.9 V showed detectable reduction peaks (arrowed in Figure 7). These results suggest that the oxidative stability limit of the material is ~3.4 V *vs.* In/InLi (~4 V *vs.* Li$^+$/Li).
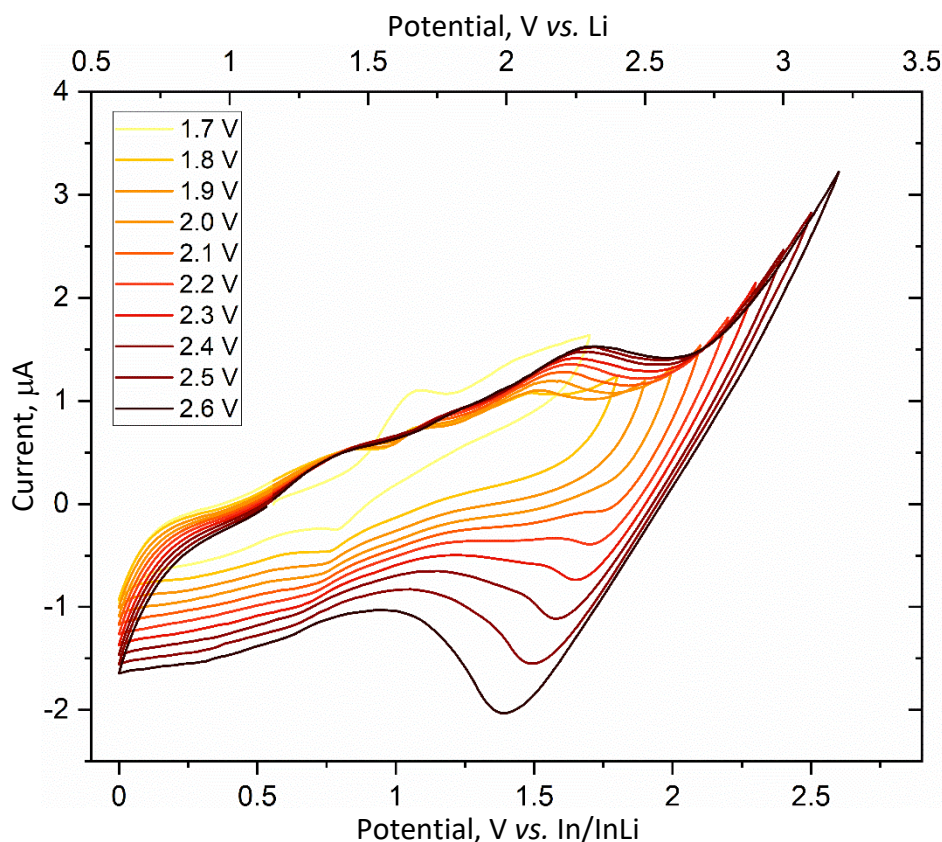
Figure 5. *Stepwise cyclic voltammograms (0.1 mV s^{-1}) for Li$_3$PS$_4$ (LPS) at 80 °C, employing the In/LPOS/LPS-C cell and oxidative potential limits of 1.7-2.6 V*
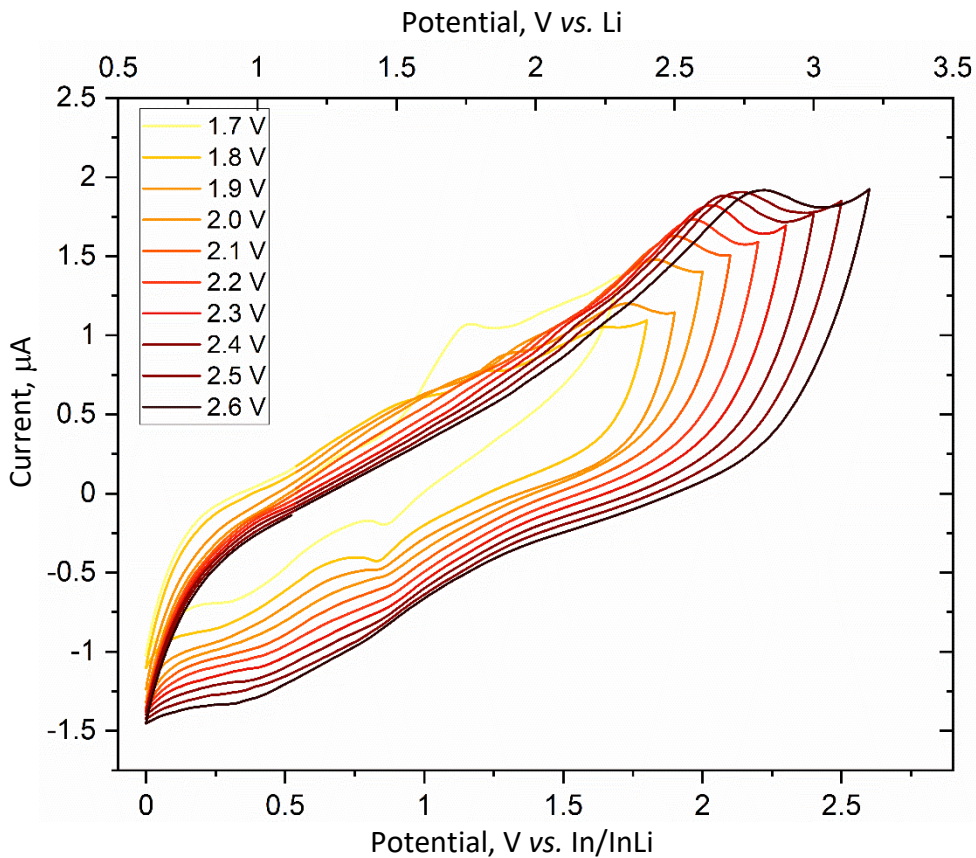
Figure 6. *Stepwise cyclic voltammograms (0.1 mV s⁻¹) for LPOS at 80 °C, employing the In/LPOS/LPOS-C cell and oxidative potential limits of 1.7 to 2.6 V*
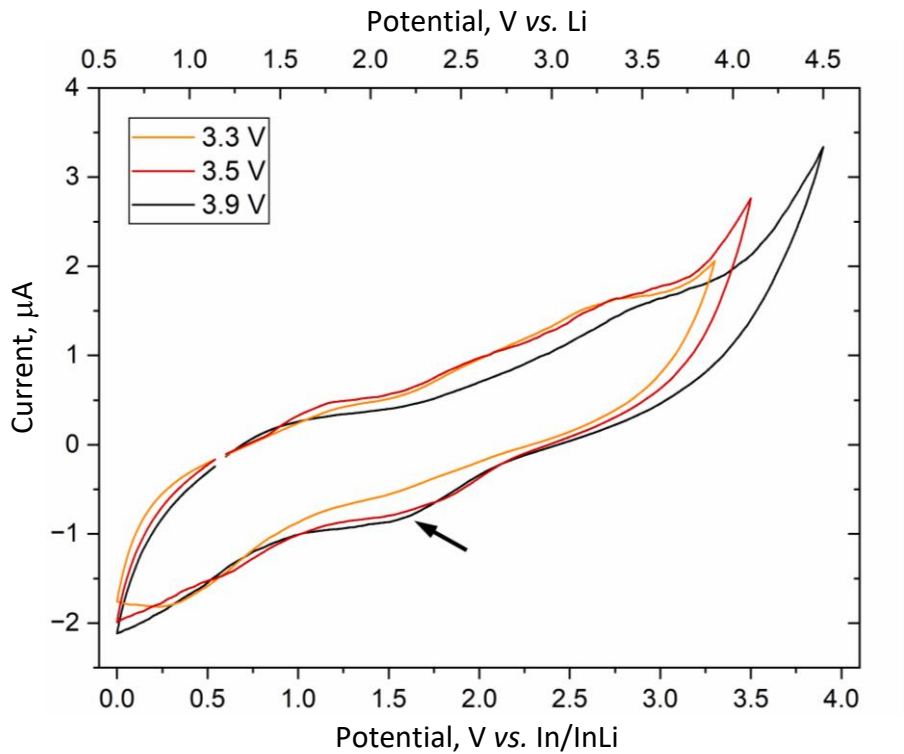
Figure 7. *Stepwise cyclic voltammograms (0.1 mV s⁻¹) for LPOS at 80 °C, employing the In/LPOS/LPOS-C cell and oxidative potential limits of 3.3 to 3.9 V*

Conclusions

A sonication-assisted liquid-phase synthesis approach is used to achieve sulfur-doping in γ-type Li_3PO_4. XRD, EDX and FTIR studies indicated that the material, after calcination at 400 °C in argon, is composed of a sulfur-doped γ-type Li_3PO_4 phase (LPOS) and a secondary phase of Li_3PO_4. The material retained deformability after sintering at 400 °C, which allowed the densification of the material by cold-pressing. Cold-pressed pellets of the material showed ion conductivity four orders of magnitude higher than that of the parent γ-type Li_3PO_4 compound. The ion conductivity of the material at 90°C is 10^{-6} S cm^{-1} with an activation energy of ion transport of 0.40(8) eV, compared with $\sim$$10^{-10}$ S cm^{-1} and 1.1 eV for parent Li_3PO_4. Enhanced ion transport properties and deformability make the material more suitable for bulk-type all-solid-state battery applications than other doped Li_3PO_4 ceramics. A mixed sulfide-oxide anion lattice in sulfur-doped Li_3PO_4 enabled better electrochemical stability towards oxidation compared with sulfide-based materials. Stepwise cyclic voltammetry studies on sulfur-doped Li_3PO_4 and Li_3PS_4 revealed enhanced electrochemical stability of sulfur-doped Li_3PO_4 against oxidation in contact with carbon (up to $\sim$4 V *vs*. Li$^+$/Li), which makes the material more suitable for application in Li-S batteries than Li_3PS_4. More studies are underway to develop optimized synthetic approaches to enhance the phase homogeneity of sulfur-doped Li_3PO_4 materials.

Conflicts of interest: There are no conflicts of interest to declare.

References

[1] J. Janek, W. G. Zeier, A solid future for battery development, *Nature Energy* **1** (2016) 16141. https://doi.org/10.1038/nenergy.2016.141

[2] J. Janek, W. G. Zeier, Challenges in speeding up solid-state battery development, *Nature Energy* **8** (2023) 230-240. https://doi.org/10.1038/s41560-023-01208-9.

[3] Y. Zhu, X. He, Y. Mo, Origin of Outstanding Stability in the Lithium Solid Electrolyte Materials: Insights from Thermodynamic Analyses Based on First-Principles Calculations, *ACS Applied Materials & Interfaces* **7** (2015) 23685-23693. https://doi.org/10.1021/acsami.5b07517

[4] T. Thompson, S. Yu, L. Williams, R. D. Schmidt, R. Garcia-Mendez, J. Wolfenstine, J. L. Allen, E. Kioupakis, D. J. Siegel, J. Sakamoto, Electrochemical Window of the Li-Ion Solid Electrolyte $Li_7La_3Zr_2O_{12}$, *ACS Energy Letters* **2** (2017) 462-468. https://doi.org/10.1021/acsenergylett.6b00593

[5] C. Wang, K. Fu, S. P. Kammampata, D. W. McOwen, A. J. Samson, L. Zhang, G. T. Hitz, A. M. Nolan, E. D. Wachsman, Y. Mo, V. Thangadurai, L. Hu, Garnet-Type Solid-State Electrolytes: Materials, Interfaces, and Batteries, *Chemical Reviews* **120** (2020) 4257-4300. https://doi.org/10.1021/acs.chemrev.9b00427

[6] K. Suzuki, M. Kamiya, N. Matsui, S. Hori, M. Hirayama, R. Kanno, Synthesis and Electrochemical Properties of Quaternary and Quinary γ-Li_3PO_4-Type Materials: Effects of Compositional Complexity in Lithium Superionic Conductors, *Journal of Physical Chemistry C* **127** (2023) 10947-10952. https://doi.org/10.1021/acs.jpcc.3c01765

[7] H. El-Shinawi, E. J. Cussen, S. A. Cussen, Morphology-controlled synthesis of novel nanostructured $Li_4P_2O_7$ with enhanced Li-ion conductivity for all-solid-state battery applications, *Dalton Transactions* **53** (2024) 4139-4146. https://doi.org/10.1039/D3DT04377K

[8] H. El-Shinawi, E. J. Cussen, S. A. Cussen, A new nanostructured γ-Li$_3$PO$_4$/GeO$_2$ composite for all-solid-state Li-ion battery applications, *Dalton Transactions* **53** (2024) 10666-10674. https://doi.org/10.1039/D4DT01423E

[9] G. Zhao, K. Suzuki, M. Yonemura, M. Hirayama, R. Kanno, Enhancing fast lithium ion conduction in Li$_4$GeO$_4$–Li$_3$PO$_4$ solid electrolytes, *ACS Applied Energy Materials* **2** (2019) 6608-6615. https://doi.org/10.1021/acsaem.9b01152

[10] G. Zhao, K. Suzuki, T. Seki, X. Sun, M. Hirayama, R. Kanno, High lithium ionic conductivity of γ-Li$_3$PO$_4$-type solid electrolytes in Li$_4$GeO$_4$–Li$_4$SiO$_4$–Li$_3$VO$_4$ quasi-ternary system, *Journal of Solid State Chemistry* **292** (2020) 121651. https://doi.org/10.1016/j.jssc.2020.121651

[11] G. Zhao, K. Suzuki, T. Okumura, T. Takeuchi, M. Hirayama, R. Kanno, Extending the Frontiers of Lithium-Ion Conducting Oxides: Development of Multicomponent Materials with γ-Li$_3$PO$_4$-Type Structures, *Chemistry of Materials* **34** (2022) 3948-3959. https://doi.org/10.1021/acs.chemmater.1c04335

[12] R. Kanno, T. Hata, Y. Kawamoto, M. Irie, Synthesis of a new lithium ionic conductor, thio-LISICON–lithium germanium sulfide system, *Solid State Ionics* **130** (2000) 97-104. https://doi.org/10.1016/S0167-2738(00)00277-0

[13] R. Kanno, M. Murayama, Lithium ionic conductor thio-LISICON: the Li$_2$S–GeS$_2$–P$_2$S$_5$ system, *Journal of The Electrochemical Soc*iety **148** (2001) A742. https://doi.org/10.1149/1.1379028

[14] X. Wang, R. Xiao, H. Li, L. Chen, Oxygen-Driven Transition from Two-Dimensional to Three-Dimensional Transport Behaviour in β-Li$_3$PS$_4$ Electrolyte, *Physical Chemistry Chemical Physics* **18** (2016) 21269-21277. https://doi.org/10.1039/C6CP03179J

[15] S. Banerjee, M. L. Holekevi Chandrappa, S. P. Ong, Role of Critical Oxygen Concentration in the β-Li$_3$PS$_{4-x}$O$_x$ Solid Electrolyte, *ACS Applied Energy Materials* **5** (2022) 35-41. https://doi.org/10.1021/acsaem.1c03795

[16] N. J. J. De Klerk, E. Van Der Maas, M. Wagemaker, Analysis of Diffusion in Solid-State Electrolytes through MD Simulations, Improvement of the Li-Ion Conductivity in β-Li$_3$PS$_4$ as an Example, *ACS Applied Energy Materials* **1** (2018) 3230-3242. https://doi.org/10.1021/acsaem.8b00457

[17] K. Takada, M. Osada, N. Ohta, T. Inada, A. Kajiyama, H. Sasaki, S. Kondo, M. Watanabe, T. Sasaki, Lithium ion conductive oxysulfide, Li$_3$PO$_4$–Li$_3$PS$_4$, *Solid State Ionics* **176** (2005) 2355-2359. https://doi.org/10.1016/j.ssi.2005.03.023

[18] K. Suzuki, M. Sakuma, S. Hori, T. Nakazawa, M. Nagao, M. Yonemura, M. Hirayama, R. Kanno, Synthesis, structure, and electrochemical properties of crystalline Li–P–S–O solid electrolytes: Novel lithium-conducting oxysulfides of Li$_{10}$GeP$_2$S$_{12}$ family, *Solid State Ionics* **288** (2016) 229-234. https://doi.org/10.1016/j.ssi.2016.02.002

[19] A. Neveu, V. Pelé, C. Jordy, V. Pralong, Exploration of Li–P–S–O composition for solid-state electrolyte materials discovery, *Journal of Power Sources* **467** (2020) 228250. https://doi.org/10.1016/j.jpowsour.2020.228250

[20] M. J. Deck, P. Chien, T. P. Poudel, Y. Jin, H. Liu, Y. Hu, Oxygen-Induced Structural Disruption for Improved Li$^+$ Transport and Electrochemical Stability of Li$_3$PS$_4$, *Advanced Energy Materials* **14** (2023) 2302785. https://doi.org/10.1002/aenm.202302785

[21] A. Miura, N. C. Rosero-Navarro, A. Sakuda, K. Tadanaga, N. H. H. Phuc, A. Matsuda, N. Machida, A. Hayashi, M. Tatsumisago, Liquid-phase syntheses of sulfide electrolytes for all-solid-state lithium battery, *Nature Reviews Chemistry* **3** (2019) 189-198. https://doi.org/10.1038/s41570-019-0078-2

[22] Z. Liu, W. Fu, E. A. Payzant, X. Yu, Z. Wu, N. J. Dudney, J. Kiggans, K. Hong, A. J. Rondinone, C. Liang, Anomalous High Ionic Conductivity of Nanoporous β-Li$_3$PS$_4$, *Journal of the American Chemical Society* **135** (2013) 975-978. https://doi.org/10.1021/ja3110895

[23] A. L. Santhosha, L. Medenbach, J. R. Buchheim, P. Adelhelm, The indium-lithium electrode in solid-state lithium-ion batteries: Phase formation, redox potentials, and interface stability. *Batteries & Supercaps* **2** (2019) 524-529. https://doi.org/10.1002/batt.201800149

[24] J. Li, W. Liu, X. Zhang, Y. Ma, Y. Wei, Z. Fu, J. Li, Y. Yan, Heat treatment effects in oxygen-doped β-Li$_3$PS$_4$ solid electrolyte prepared by wet chemistry method, *Journal of Solid State Electrochemistry* **25** (2021) 1259-1269. https://doi.org/10.1007/s10008-021-04904-2

[25] B. Wang, B. C. Chakoumakos, B. C. Sales, B. S. Kwak, J. B. Bates, Synthesis, crystal structure and ionic conductivity of polycrystalline lithium phosphorous oxynitride with the γ-Li$_3$PO$_4$ structure, *Journal of Solid State Chemistry* **115** (1995) 313-323. https://doi.org/10.1006/jssc.1995.1140

[26] C. F. Holder, R. E. Schaak, Tutorial on powder X-ray diffraction for characterizing nanoscale materials. *ACS Nano* **13** (2019) 7359-7365. https://doi.org/10.1021/acsnano.9b05157

[27] C. Sourisseau, R. Cavagnat, M. Fouassier, R. Brec, S.H. Elder, Infrared, Raman, resonance Raman spectra and lattice dynamics calculations of the solid potassium(I) nickel(II) thiophosphate compound, KNiPS$_4$, *Chemical Physics* **195** (1995) 351-369. https://doi.org/10.1016/0301-0104(95)00083-Z

[28] K. Nakamoto, in: *Infrared and Raman spectra of inorganic and coordination compounds*, 4th Ed., Wiley-Interscience, Chinchester, 1986.

[29] D. E. C. Corbridge, E. J. Lowe, The infra-red spectra of some inorganic phosphorus compounds, *Journal of the Chemical Society* (1954) 493-502. https://doi.org/10.1039/JR9540000493

[30] J. T. S. Irvine, D. C. Sinclair, A. R. West, Electroceramics: Characterization by Impedance Spectroscopy, *Advanced Materials* **2** (1990) 132-138. https://doi.org/10.1002/adma.19900020304

[31] S. Muy, J. C. Bachman, H. H. Chang, L. Giordano, F. Maglia, S. Lupart, P. Lamp, W. G. Zeier, Y. Shao-Horn, Lithium conductivity and Meyer-Neldel rule in Li$_3$PO$_4$-Li$_3$VO$_4$-Li$_4$GeO$_4$ lithium superionic conductors, *Chemistry of Materials* **30** (2018) 5573-5582. https://doi.org/10.1021/acs.chemmater.8b01504

[32] G. F. Dewald, S. Ohno, M. A. Kraft, R. Koerver, P. Till, N. M. Vargas-Barbosa, J. Janek, W. G. Zeier, Experimental Assessment of the Practical Oxidative Stability of Lithium Thiophosphate Solid Electrolytes, *Chemistry of Materials* **31** (2019) 8328-8337. https://doi.org/10.1021/acs.chemmater.9b01550

[33] F. Han, Y. Zhu, X. He, Y. Mo, C. Wang, Electrochemical Stability of Li$_{10}$GeP$_2$S$_{12}$ and Li$_7$La$_3$Zr$_2$O$_{12}$ Solid Electrolytes, *Advanced Energy Materials* **6** (2016) 1501590. https://doi.org/10.1002/aenm.201501590